Quantum exciton solid in bilayer two-dimensional electron-hole systems

S. T. Chui,[1] Ning Wang,[2] and Chun Yu Wan[2]
[1]*Bartol Research Institute and Dept. of Physics and Astronomy, University of Delaware, Newark, Delaware 19716, USA*
[2]*Department of Physics, Hong Kong University of Science and Technology, Clear Water Bay, Hong Kong*

(Received 7 May 2020; revised 20 August 2020; accepted 21 August 2020; published 15 September 2020)

We propose a state of excitonic solid for bilayer two-dimensional electron-hole systems in transition metal dicalcogenides stacked on opposite sides of thin layers of BN. Properties of the exciton lattice are studied. We found that for the experimental parameters of interest, the solid by itself will melt. However, the solid can be stabilized by the potential due to the BN. We studied the possible manifestation of supersolid behavior due to quautum transport of defects and found that it is manifested as an approximately quantized conductance in Coulomb drag measurements.

DOI: 10.1103/PhysRevB.102.125420

I. INTRODUCTION

There has been much recent interest recently in bilayer electron-electron (e-e) and electron-hole (e-h) in graphene and transition metal dicalcogenides (TMDC) systems. This follows earlier interest in the physics of the two-dimensional electron gas in single and double layers in Si-MOSFET and in GaAs heterostructures [1]. For a single layer, the electrons are expected to be a fluid at high densities and a solid at low densities [2]. For the bilayer electron-hole system, there has been much interest in the possibility that the electron and hole forming an exciton which then Bose condense into a superfluid [3]. This is usually expected in the limit with the exciton size less than the average interparicle spacing so that the identity of the exciton is well defined. The possibility of a condensate of excitons has recently been discussed in graphene [4] and in TDMC systems [5]. Wang and coworkers [5] present optical evidence for the existence of excitons in TMDC bilayers but no transport measurement have been carried out. There has not been much study on the possibility of the excitons forming a quantum solid instead of a Bose fluid. A boson can in principle exhibit both phases, as is exemplified by the example ^{4}He, which can exist in both a solid and a superfluid phase. The energetics of this exciton solid is different from that of the Wigner crystal, which is predicted to be stable at low densities ν. At large distances, the excitons interact with each other with dipolar interactions, much weaker than the Coulomb interaction of the electron solid. The potential energy gained per particle is proportional to $-\nu^{3/2}$ and cannot overcome the increase in the quantum kinetic energy which is manifested as the zero point energy of the phonons that is proportional to $\nu^{5/4}$. The quantum exciton solid by itself is thus not stable at low density. Suris [6] considered the phase boundary between the exciton gas and the exciton solid in the classical limit at low density. In the solid energy, he only included the potential energy gained but not the zero point energy of the phonons. In this paper, we study the physical properties of the quantum exciton solid.

Monolayer graphene exhibit a linear dispersion near the Fermi energy and the physics is different from those with parabolic particle bands, which are exhibied by two classes of experimental systems under active study at the moment. These are double layer graphene and double layer TMDC system sandwiching a BN layer. The effective masses of the particles in the double layer graphene ($0.03m_e$)[7] is much smaller than that in the TMDC (for WSe_2, we have used a hole mass of $0.85m_e$, an electron mass of 0.5 with a reduced mass of $\mu = 0.31$) [8]. The thin BN layer is of thickness $d \approx 5$ nm [9] so that the electrons and holes in layers on opposite sides of BN have a separation larger than d. Following our previous work on the phonons of rare gases adsorbed on graphite [10], we carried out self-consistent phonon calculation of the excitonic solid system. A criterion of the stability of the solid is the Lindemann ratio, usually defined as the root mean square lattice vibration normalized by the lattice constant. In two dimension the root mean square vibration can be infinite. A useful alternative is to focus on the relative vibration between nearest neighbors. For quantum melting, the melting point occurs when this ratio is about 10% [2]. We found that for current experimental parameters, the Lindemann ratio for TMDC is about 20%; for double layer graphene, 63%. However, the excitons are in the presence of the BN layer. There is charge transfer between Boron and Nitrogen of about $Q \approx 0.47$ in BN [11]. We study the phonon in the presence of the external potential due to BN and show the Lindemann ratio can be changed. We found that the Lindemann ratio is reduced to 7% for TMDC and 27% for bilayer graphene. This suggests that such an excitonic solid state is indeed possible for current experimental system with TMDC layers.

Supersolid behavior has been discussed for Boson solids such as solid ^{4}He [12]. We discuss the possible manifestation of this kind of behavior for the current system. We found that it is manifested as an approximately quantized conductance in the Coulomb drag measurement which we have recently observed [13] and which motivated the current work.

II. EXCITON IN THE DOUBLE LAYER STRUCTURE

To gain some intuition of the properties of the system, we first discuss the physical property of a single exciton in the bilayer structure with BN in between. We describe the screening of the Coulomb potential V_0 by a semiconductor film of thickness d_1 and anisotropic dielectric constants ϵ_{xy}, ϵ_z in Appendix A. Solutions with the charge inside the film has been applied to the study of excitons in layered structures with isotropic dielectric constants [14,15]. They focus on the limit so that the thickness of the film is less than the transverse dimension. We found that the screened potential for the interaction at transverse distance r becomes

$$V(r, d_1) = \int d^2q dq_z e^{iq_z d_1 + iq\cdot r} V_0(q, q_z)/\epsilon_{\text{eff}},$$

where the effective dielectric constant is given by

$$1/\epsilon_{\text{eff}} = (1-\beta^2)/(1-\beta^2 e^{-2\gamma q d_1}), \tag{1}$$

$\gamma = (\epsilon_{xy}/\epsilon_z)^{1/2}$,

$$\epsilon = \epsilon_z \gamma = (\epsilon_z \epsilon_{xy})^{1/2}, \tag{2}$$

$$\beta = (1-\epsilon)/(\epsilon+1) \tag{3}$$

is the well known image charge in elementary electrostatics [16]. q is a measure of the inverse transverse length 1/r of interest. For thin films with the transverse distance of interest larger than its thickness, $qd_1 \ll 1$, $\epsilon_{\text{eff}} \approx 1$. The TMDC films are thin and thus do not provide screening. The transverse dimension of the exciton is smaller than the BN thickness, however. Thus for the screening by the BN films, we take the approximation $2\gamma q d_1 \gg 1$. $1/\epsilon_{\text{eff}} \approx 1-\beta^2$. This limit is opposite to that focused on by Keldysh [14]. Physically, ϵ_{eff} is a product of a factor $1+\beta$ from the sum of the original charge and the image charge for the first interface and a factor $1-\beta$ from the second interface. With [17] $\epsilon_{xy} = 6.93$ and $\epsilon_z = 3.76$, we obtain $1/\epsilon_{\text{eff}} = 0.55$.

The typical size of an "ordinary" exciton is of the order of the Bohr radius. The Bohr radius for the graphene system ($a_{\text{B,graphene}} = 90$ Å) is usually larger than the BN layer thickness d. The Bohr radius for the TMDC system $a_{\text{B,TMDC}} = 3$ Å. This exciton size is smaller than the thickness of the BN layer, however. The exciton binding energy for the double layer graphene system is of the order Ryberg $\mu/m_e/\epsilon^2 = 137$ K. For double layer TMDC, the conventional formula gives a binding energy more than twenty times larger. It is much more difficult to ionize them. However, the exciton in the TMDC system needs to be reexamined since the Bohr radius is now less than the BN layer thickness. The motion of the electron-hole system is now two-dimensional. We discuss this next.

The transverse separation r of the two-dimensional exciton is of the order of the Bohr radius between the electron and the hole in the TMDC and is much less than their vertical spacing d_1. The Coulomb potential energy between the electron and the hole can be expanded as a power series in r/d_1 as

$$V = -e^2(r^2+d_1^2)^{-1/2} \approx -e^2/d_1 + e^2 r^2/d_1^3/2. \tag{4}$$

$e^2 = q_e^2(1-\beta^2)/(4\pi\epsilon_0)$. In this approximation, the exciton wave function is that of a two-dimensional harmonic oscillator with a force constant $k = e^2/d_1^3 = \mu\omega^2$ and $\omega = [e^2/d_1^3/\mu]^{1/2}$. The exciton binding energy is $E_{\text{ex}} = -e^2/d_1 + \hbar\omega/2$. This can be written as

$$E_{\text{ex}} = e^2/d_1[-1 + (a_B/d_1)^{1/2}/2]. \tag{5}$$

For TMDC with $d_1 = 50$ Å, $(1-\beta^2) = 0.55$, $E_{\text{ex}} = 1839.1$ K.

The size of the exciton is $\xi = [\hbar/(\mu\omega)]^{1/2}$. Thus $\xi/d_1 \approx (a_B/d_1)^{1/4} \approx 0.46$. For current experimental parameters, $\xi \approx 23$ Å. The expansion parameter in Eq. (4) $(\xi/d_1)^2 \approx 1/4$. This provides for a justification of our harmonic expansion. In this paper, we are interested in exciton densities so that the average interexciton distance a is of the order of 100 Å. The exciton size ξ is less than a. Thus the condition of well defined excitons is satisfied.

The electroluminence is proportional to the probability of finding the electron and hole on top of each other and thus proportional to $\psi_{\text{ex}}(r=0) \propto 1/\xi^2$.

III. EXCITON SOLID PHONONS: OPTICAL AND ACOUSTIC MODE

We next examine the phonon excitations when the excitons are arranged in a lattice. We ignore the motion of the particles perpendicular to the layer and focus on their in plane motion. The lattice motion of the exciton solid consists of two modes, an optic mode from the intraexciton vibration and an acoustic mode from the interexciton vibration. We separate the optical mode from the acoustic mode as follows. We assume the lattice positions to be at $\mathbf{R}_i$. At each site, we write the in plane coordinates of the electrons and holes in terms of the center of mass equilibrium and fluctuation positions ($\mathbf{R}_i + \delta\mathbf{R}$) and the relative ($\mathbf{r}_i$) coordinates so that the coordinate of the i$^{\text{th}}$ electron is given by $\mathbf{r}_{ei} = \mathbf{R}_i + \delta\mathbf{R}_i + \mathbf{r}_i/2$; of the hole, $\mathbf{r}_{hi} = \mathbf{R}_i + \delta\mathbf{R}_i - \mathbf{r}_i/2$. The potential energy of interaction involves $U = \sum_{\alpha,\beta=e,h,i,j} V[(r_{\alpha,i} - r_{\beta,j})^2 + d^2\delta_{\alpha,\beta}]^{1/2}/2$ where $V(u) = e^2/(\epsilon_{\text{eff}}u)$ is the Coulomb potential. We are interested in the interexciton interaction at transverse distances larger than the lattice spacing that is of the order of 100 Å and thus are larger than the BN thickness $d \approx 50$ Å. We thus have assumed $\epsilon_{\text{eff}} \approx 1$. We expand the interaction in powers of δR_i and r_i. Since U is even in r_i, only even powers of this quantity appears in a power series expansion. Thus in the phonon approximation when the second order terms are kept we get $U = \sum_{i\neq j}(\delta R_i - \delta R_j)^2 \cdot \nabla\nabla V_{ij} + \sum_{i,j}(r_i - r_j)^2 \cdot \nabla\nabla V_{ij}$. The two degrees of freedom are decoupled. For the relative coordinate, there is an additional intraexciton interaction for $i = j$ in the sum for U. Following our previous work on the phonons of rare gases adsorbed on graphite [10], we carried out self-consistent phonon calculation of this bilayer system. The harmonic frequency is obtained from solving the phonon equation for the Fourier transform phonon modes:

$$m\omega^2 e_i(q) = \sum_j e_j(q) D_{ij}(q), \tag{6}$$

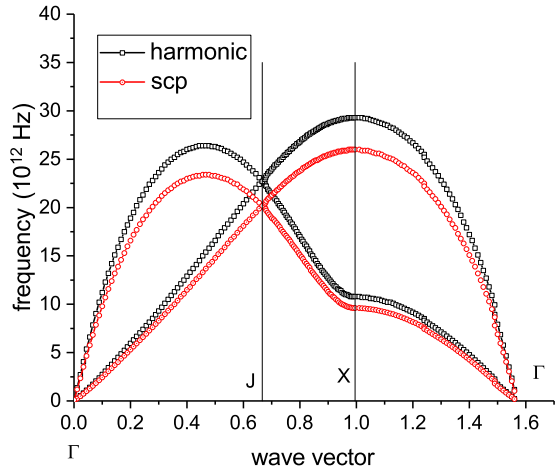

FIG. 1. Phonon energy for the center of mass along symmetry directions of the two-dimensional Brillouin zone for $r_s = 13.3$, corresponding to a density of 2×10^{12} cm^{-2}.

where the dynamical matrix $D_{ab}(q) = \sum_{\mathbf{R}}(1 - \cos \mathbf{q} \cdot \mathbf{R})$ $\nabla_a \nabla_b U(R)$, $e_i(q)$ is the polarization vector. The harmonic acoustic center of mass phonon frequencies for an triangular exciton lattice for parameters of our recent experiments(density 2×10^{12} cm^{-2} lattice spacing 71 Å) are shown in Fig. 1 as a function of the wave vector along symmetry directions.

Also shown in this figure are the self-consistent phone frequencies obtained by replacing the dynamical matrix D by an average $\langle D \rangle$ so that $\langle D_{ab}(q) \rangle = \sum_{\mathbf{R}}(1 - \cos \mathbf{q} \cdot \mathbf{R})$ $\nabla_a \nabla_b \langle U(R + \delta R) \rangle$. The angular brackets indicate a self-consistent average over the quantum fluctuation δR. The details of this is described in Appendix B.

The harmonic and the self-consistent optic exciton vibration frequencies are shown in Fig. 2 as a function of the wave vector along symmetry directions. We have explored the dependence of this on the density of the system. The harmonic and the self-consistent acoustic center of mass phonon frequencies for an triangular exciton lattice of a larger spacing

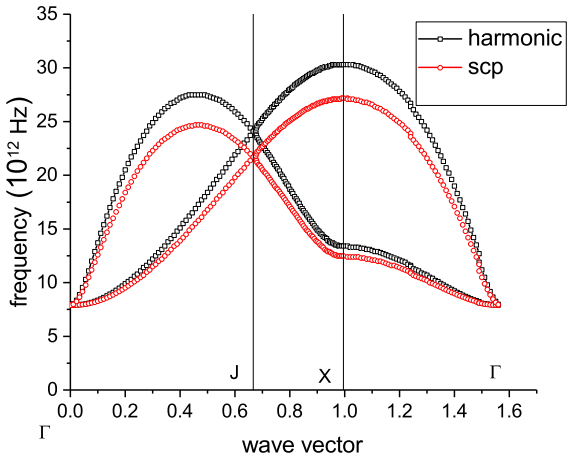

FIG. 2. Phonon energy for the intraexciton mode along symmetry directions of the two-dimensional Brillouin zone.

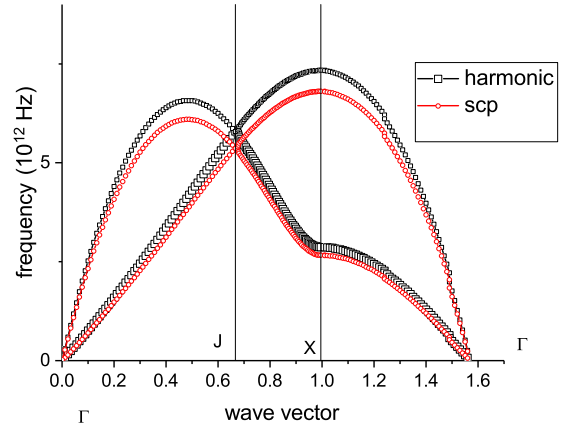

FIG. 3. Phonon energy for the acoutic mode along symmetry directions of the two-dimensional Brillouin zone. The lattice constant is twice that in the previous two figures with $r_s = 26.6$, corresponding to a density of 0.5×10^{12} cm^{-2}.

of spacing 152 Å are shown in Fig. 3 as a function of the wave vector along symmetry directions.

IV. LINDEMANN RATIO

We discuss first the qualitative behavior of the Lindemann ratio for our system. The interparticle potential has two regimes of behavior. At small (large) distances with $r \ll d (r \gg d)$, $V \approx e^2 \alpha r^{-n}$ where $n = 1$, $\alpha = 1$ ($n = 3$, $\alpha = 1/d^2$). The mean square lattice vibration is $\langle r^2 \rangle = \sum_q \hbar(2n_q + 1)/(m\omega_q)$, where n_q is the number of phonons. The Bohr radius is $a_B = \hbar^2/(me^2)$. For a general interparticle potential $V \approx e^2 \alpha r^{-n}$ the phonon frequency is given by $m\omega^2 = V'' = e^2 \alpha a^{-n-2}.\omega = e(\alpha/m)^{1/2} a^{-1-n/2}$. The Lindemann ratio at low temperatures is given by $\langle r^2 \rangle / a^2 = (a_B/\alpha)^{1/2} a^{n/2-1}$. We thus expect that at very high densities with small $a < d$, $\langle r^2 \rangle / a^2 = (a_B/a)^{1/2}$. Correspondingly at very low densities with large $a > d$, $\langle r^2 \rangle / a^2 = (a_B a)^{1/2}/d$. For both very large and very small a, the fluctuation and the Lindemann ratio is large; one has a fluid. This is in contrast with the Wigner crystal ($n = 1$) where at large a, the Lindemann ratio, $(a_B/a)^{1/2}$, is small and the solid is stable.

Our numerical result for the Lindemann ratio is shown in Fig. 4 as a function of r_s. It is around 20% and not a strong function of the density, as is indicated above.

V. EFFECT OF BN

In the two-dimensional electron system, the external static potential such as that due to the dopants can stabilize the solid phase relative to the fluid phase [18]. In the current system, there is a thin boron nitride film in the middle in the experimental systems. The two-dimensional electrons and holes see a static Coulomb potential from the periodic array of boron and nitrogen ions. We find this potential produces a significant effect in reducing the spatial fluctuation of the exciton solid and enhance its stability. We calculate this next.

There is a charge transfer between boron and nitrogen in boron nitride of magnitude [11] $|Q_{B,N}| \approx 0.47$. We calculate this potential by decomposing the potential from BN film as

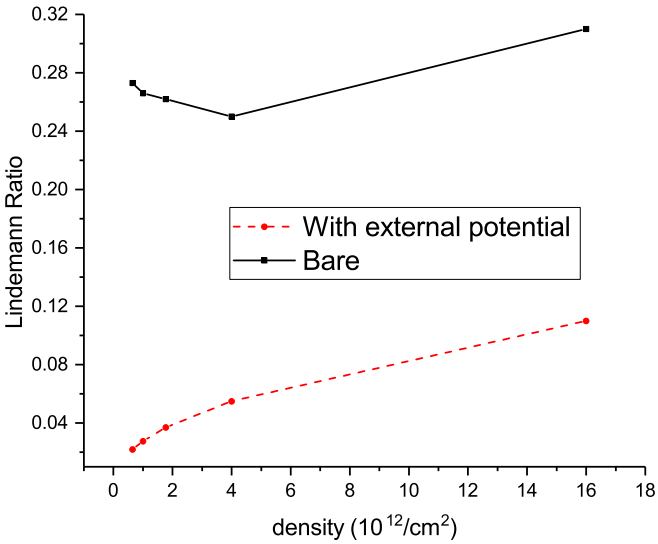

FIG. 4. The Lindemann ratio as a function of density with and without the external potential from BN.

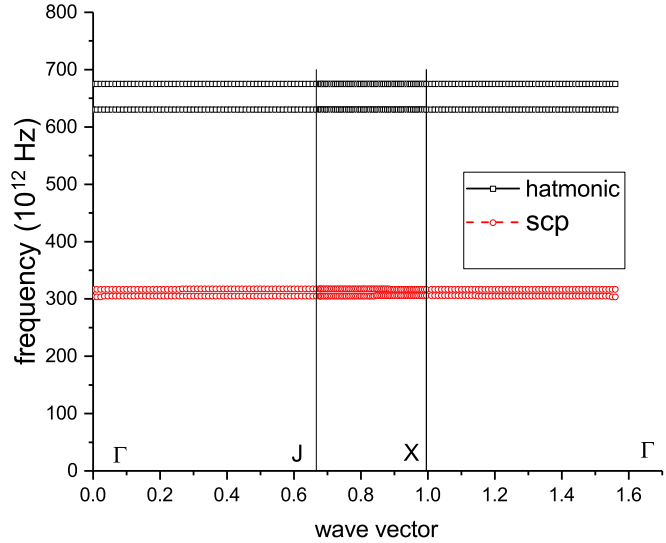

FIG. 5. Phonon energy for the center of mass along symmetry directions of the two-dimensional Brillouin zone in the presence of the external potential due to BN for a density of 2×10^{12} cm^{-2} and $\delta R_G/a_{BN} = 0.025$.

consisting of a sum of two-dimensional periodic arrays at different vertical distances h away from the two-dimensional electron (hole) gas. The potential of each two-dimensional periodic array is sum of the Coulomb potential U from the ions at the two-dimensional periodic BN lattice sites $\mathbf{R}_i^{B,N} + \delta\mathbf{R}_i^{B,N}$ with modulation $\delta\mathbf{R}_i^{B,N} = \sum_G \delta\mathbf{R}_G^{B,N} e^{i\mathbf{G}\cdot\mathbf{R}_i}$ from the interaction of the BN latice with the incommensurate TMDC lattice with reciprocal lattice vectors $\mathbf{G}$. We assume that the hole lattice is displaced by a slight amount relative to the electron lattice so that both the electron and the hole lattices are close to the minima of the periodic potential [19].

The potential from the boron ions is given by $V_B(r) = \sum_i U_B(r - \mathbf{R}_i^B - \delta\mathbf{R}^B)$. The screening of the Coulomb potential when the charge is inside the semiconductor is also discussed in Appendix A. From Eq. (A13), V_B can be written in Fourier space as $V_B(r) = \int d^2q/(2\pi)^2 \sum_i \tilde{U}_q e^{iq\cdot(r-\mathbf{R}_i^B-\delta\mathbf{R}^B)}$ where $\tilde{U}(q) = Q/\epsilon(1-\beta)\sum_h e^{-|q|h}/|q|/2$. $(1-\beta)/\epsilon = 1/\epsilon_{am}$ is the inverse of arithmatic mean of the dielectric constants on opposite sides of the interface. Because the boron and the nitrogen ions have opposite charges, we assume $\delta\mathbf{R}_G^N = -\delta\mathbf{R}_G^B$. To illustrate our result, we have used a typically small strain of $\delta\mathbf{R}_G^N/a_{BN}$ of 2.5%.

In terms of the reciprocal lattice vectors K of the BN lattice

$$V_B(r) \approx \sum_K [V_{B1}^K(r) + \sum_G V_{B2}^{K-G}(r)]. \tag{7}$$

$V_{X1}^K(r) = \tilde{U}_K e^{i\mathbf{K}\cdot\mathbf{r}}/a_c$, $V_{X2}^{K-G}(r) = i\tilde{U}_{G-K} e^{i(\mathbf{G}-\mathbf{K})\cdot\mathbf{r}}[(\mathbf{G}-\mathbf{K})\cdot\delta\mathbf{R}_G^X)]/a_c$; a_c is the area of the unit cell of the BN lattice. Because of the factor $e^{-|K|h}$ in the Fourier transform of the Coulomb potential V_B is dominated by contributions from the nearest two BN planes with $h_1 \approx 3.5$ Å, $h_2 \approx 7$ Å and from the smallest reciprocal lattice vector $K = 2\pi/a_{BN}$ and $K - G = 2\pi(1/a_{BN} - 1/a_{\mathrm{TMDC}})$.

In our self-consistent calculation, we take the average of the pinning potential from the quantum fluctuation of the position of the exciton lattice. The averages of the pinning potentials over the spatial fluctuations of the excitons are determined by the corresponding Debye-Waller factors as

$$\langle V_{Bi}^Q(r)\rangle \approx V_{Bi}^Q e^{-<(Q\cdot\delta r)^2>/2}. \tag{8}$$

In our calculation, this effect is determined self-consistently. We find that the Debye-Waller factor for V_{B1} is extremely small because $\langle(K\cdot\delta r)^2\rangle$ is large. The average pinning potential V_{B2} with a wave vector $|G-K| \approx |K|/4 < |K|$ is much bigger. Similarly the potential from the nitrogen ions at sublattice position δ is given by $V_N = -\sum_i U(r - R_i - \delta R_i^N - \delta)$, where the boron nitrogen distance is $\delta = 0.1446$ nm. This can be written as a Fourier series:

$$V_N(r) \approx -\sum_K [V_{N1}^K(r) e^{-iK\cdot\delta} + \sum_G V_{N2}^{K-G}(r) e^{-i(K-G)\cdot\delta}]. \tag{9}$$

The BN potential is incommensurate with the lattice constant of the exciton solid; misfit dislocations will form [20,21]. The lattice constant a of the exciton solid lattice is very different from that of BN potential so that $\gamma = a(G-K)/(2\pi)$ is big. We approximate γ by the closest integer γ_0. Over most $[1-(\gamma-\gamma_0)/\gamma]$ of the Brillouin zone away from the zone center, the phonons are well approximated by that of a commensurate one with periodicity $a_0 = 2\pi\gamma_0/(G-k)$ [21] so that $(a_0 - a)/a$, the difference in periodicity between the commensurate and the incommensurate case, is small. An example of the approximate phonon dispersion for the center of mass in the presence of this potential away from the zone center is shown in Fig. 5 for a density with $r_s = 13.3$ and $\delta R_G^B/a_{BN} = 0.025$ [22]. In this figure, we show both the harmonic frequency without the Debye Waller factor and the self-consistent phonon (scp) frequency where the Debye Waller factor is self-consistently determined. The contribution from $V_{BN,1}$ is significant in the harmonic approximation and becomes very small in the scp result.

Relative to the bare phonon frequency, the phonon frequency with the pinning potential from BN is increased and the lattice vibration amplitude is reduced. The Lindemann

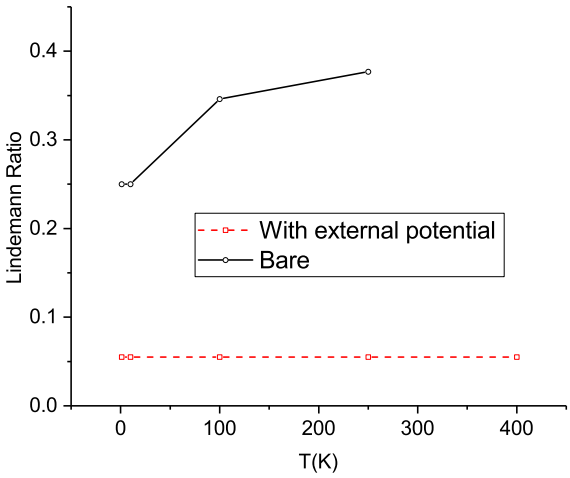

FIG. 6. The Lindemann ratio as a function of temperature a density of 4×10^{12} cm^{-2} with and without the external potential from BN.

ratio for the exciton solid in the presence of this potential is shown in Fig. 4 as a function of the density of the system. This factor is now less than around ten% and suggests that the solid can be stabilized by the BN potential. The temperature dependence of this ratio is shown in Fig. 6 a density of 4×10^{12} cm^{-2}. This suggests that the solid is stable at low temperatures.

VI. POSSIBLE "SUPERSOLID" BEHAVIOUR

There has been much recent interest in the supersolid behavior of Boson solids such as ^{4}He [12]. This kind of phenomenon is believed to come from the quantum transport of defects. In our system the defect energy is lower at the edge so we expect the density of defects to be higher there. Thus we expect the possible "supersolid" behavior to be dominated by the one dimensional quantum transport of defects at the edges. There has been much interest in the quantum transport of electrons in wires [23], which manifested in a conductance of the order of $G_0 = 2e^2/h$. In one dimension there is no difference in the properties of the current carrying single particle excitations between impenetrable bosons and fermions [24]. We thus expect a similar conductance to be manifested in the Coulomb drag measurement, which we have recently observed [13] and which motivated the current work.

VII. CONCLUSION

In conclusion, we examine a collection of excitons for the limit that the exciton size is less than the exciton separation so that the excitons are not interpenetrating. We propose that a collection of these excitons can also form a solid in addition to being a fluid. The stability of this in TMDC bilayer systems is investigated. The external potential from the BN substrate is found to be important and can stabilize the solid phase. Our description for the exciton solid differs from that for the other limit when the excitons size is larger than the exciton separation. In that case, the excitons are interpenetrating and their identity is not well defined. This other limit also corresponds to the charge density wave [25]/excitonic insulator [26], which is usually described by a generalization of the mean field BCS type wave function $\Pi(u_k - v_k b^+_{k+Q} a_k)|0>$ for electron (hole) operators b^+_p (a_q) and coefficients u and v. In real space, this function Ψ is a "Slater determinant" of particle hole functions $f(r_e - r_h)$ with specific two body momentum correlations [27]: $\Psi = \sum_{P,Q}(-1)^{P+Q}\Pi_{i,j} f(r_{ePi} - r_{hQj})$ where we sum over all permutations P and Q of the particle and hole indices. The order parameter in this limit is $\langle \rho_q \rangle = \langle \sum_p b^+_{p+q} a_p \rangle$, the average charge density of specific momentum q. The stability of this phase comes from the nesting of Fermi surfaces of particle and hole bands with momentum difference q so that the kinetic energy cost of forming an exciton is particularly small. This nesting of Fermi surfaces is absent in the bilayer TMDC system.

The electron-hole system can also exist in a metallic state of an electron-hole plasma, as has been observed in bulk Ge under laser excitation [28,29]. We have explored such a state for the current system with fixed node quantum Monte Carlo simulation [30] and found that for a single valley spin polarized system, the metallic state is more favorable for $r_s < 5$ for the bilayer system. This is more likely to be observed in bilayer graphene. For the similar density, the corresponding r_s is much smaller because of a much higher Bohr radius in the graphene system.

The band structure of incommensurate graphene on hBN were studied by Jung and coworkers [31] using a Hamiltonian with parameters extracted from calculations using the local density approximation, which assumes metallic screening so that the potential from the boron and nitrogen ions are short-ranged. We are interested in a different class of problem. We focus on the Coulomb interaction between the electrons in the TDMC and the boron and nitrogen ions in BN, we have used a long-range Coulomb potential for the interaction. There is no metallic screening since BN is a semiconductor and the exciton solid is an insulating state.

Even though there is no long-range order due to thermal fluctuation at finite temperature in two dimension, a solid phase with finite shear modulus still exist. Kosterlitz and Thouless [32] proposed that the melting transition to a fluid with zero shear modulus occurs when the free energy of a dislocation becomes zero. This idea can be generalized to quantum melting at zero temperature if one includes the change in the zero point phonon field energy when a dislocation is created [33]. Calculations with this idea provides good agreement for the melting boundary of the Wigner crystal at zero temperature. We hope to explore if this is applicable to the present case.

ACKNOWLEDGMENT

N. Wang thanks the support from the Research Grants Council of Hong Kong (Project No. 16300717).

APPENDIX A: SCREENING OF A CHARGE BY AN ANISOTROPIC DIELECTRIC FILM

Here we describe the solution of the electrostatics problem of a point charge on top of a cylindrically symmetric

anisotropic dielectric film between $z = d_1$ and $z = 0$ and dielectric constants ϵ_z and ϵ_{xy}. The physics of representing the induced polarization charge density at the interface by the method of images is well known [16]. Solutions with the charge inside the film has been applied to the study of excitons in layered structures with isotropic dielectric constants [14,15]. The effect of images in an anisotroic system for a single interface was discussed by Mele [34].

We separate the space into three regions, middle (m) with $0 < z < d_1$, up (u) with $z > d_1$ and down (d) with $z < 0$. We assume that there is a charge of magnitude $4\pi\epsilon_0 Q$ at a height $d > d_1$ and solve the problem by matching the tangential (normal) components of the electric (displacement) fields at the interfaces. This is an alternative formulation of the usual method of summing the geometric series of the potential from an infinite number of images that captures the induced polarization at the interfaces. We write the electrostatic potentials at transverse position r and height z in the u and d regions as

$$V^u(r,z) = \int d^2q/(2\pi)^2 e^{iq\cdot r}[Qe^{-q|d-z|} + G'e^{-q(z-d_1)}]/q/2,$$

$$V^d(r,z) = \int d^2q/(2\pi)^2 V_s(q) e^{(qz+iq\cdot r)}/q/2.$$

V_s is the potential "screened" by the film that we are looking for. The general form for the electrostatic potential in an anisotropic material is given by

$$\int d^2q dq_z e^{i(\pm q_z z + q\cdot r)}/(\epsilon_{xy}q^2 + \epsilon_z q_z^2)/(2\pi)^3. \tag{A1}$$

After performing the q_z integration we obtain a general expression for the potential in the middle:

$$V^m(r,z) = \int d^2q/(2\pi)^2[F(q)e^{-\gamma qz} + F'(q)e^{\gamma qz}]e^{iq\cdot r}/q/2,$$

where $\gamma = (\epsilon_{xy}/\epsilon_z)^{1/2}$

We first consider the interface at $z = 0$. From the continuity of E_{xy}, we get

$$F + F' = V_s. \tag{A2}$$

From the continuity of the normal component of the displacement field D_z, we get

$$\epsilon(-F + F') = V_s, \tag{A3}$$

where $\epsilon = \epsilon_z\gamma = (\epsilon_z\epsilon_{xy})^{1/2}$. Combining with Eq. (A2), we get

$$F + F'\beta = 0. \tag{A4}$$

$\beta = (1-\epsilon)/(\epsilon+1)$ is the usual expression for the induced image charge. We next look at the interface at $z = d_1$. From the continuity of E_{xy},

$$Fe^{-\gamma qd_1} + F'e^{\gamma qd_1} = Q'' + G', \tag{A5}$$

$Q'' = Q\exp[-q(d-d_1)]$. From the continuity of D_z, we get

$$\epsilon(-Fe^{-\gamma qd_1} + F'e^{\gamma qd_1}) = Q'' - G'. \tag{A6}$$

From these we get

$$\beta Fe^{-\gamma qd_1} + F'e^{\gamma qd_1} = Q''(1+\beta). \tag{A7}$$

Using Eq. (A4) $F' = Q''(1+\beta)/(e^{\gamma qd_1} - \beta^2 e^{-\gamma qd_1})$. We finally get the result for the net "screened" potential

$$V_s = F + F' = Qe^{-\gamma qd}/\epsilon_{\rm eff},$$

where the effective screening constant is now given by

$$1/\epsilon_{\rm eff} = (1-\beta^2)/(1-\beta^2 e^{-2\gamma qd_1}), \tag{A8}$$

$$Fe^{-\gamma qd_1}(1+\epsilon) + F'e^{\gamma qd_1}(1-\epsilon) = 2G',$$

$$Q''/(1-\beta)/\epsilon_{\rm eff}[-\beta e^{-2\gamma qd_1}(1+\epsilon) + (1-\epsilon)] = 2G',$$

$$Q''2(1-\beta^2)/\epsilon_{\rm eff}[-\beta e^{-2\gamma qd_1} + \beta] = 2G',$$

$$Qe^{-q(d-d_1)}\beta(1-e^{-2\gamma qd_1})/(1-\beta^2 e^{-2\gamma qd_1}) = G'.$$

For a very thin layer when the transverse length scale of interest is much larger than the thickness, $qd_1 \ll 1$, $\epsilon_{\rm eff} = 1$. Very thin dielectric film provides no screening, as we expect. For the case when the transverse length scale is less than the film thickness, $qd_1 \gg 1$, $1/\epsilon_{\rm eff} \approx (1-\beta^2)$. This is a product of screening factors of $1+\beta$ and $1-\beta$ from the top and bottom interfaces. For BN, $\epsilon = (6.93 \times 3.76)^{1/2} = 5$, 1, $\beta = 0.67$, and $1-\beta^2 = 0.55$.

In real space,

$$V^d(r,z) = Q(1-\beta^2)\int dqJ_0(qr)/(4\pi) \times e^{q(z-\gamma d)}/(1-\beta^2 e^{-2\gamma qd_1}).$$

1. Charge in the middle

This section describes what happens when the charge is in the middle. We consider a slight generalization so that the dielectric constants of the top and bottom are ϵ_u and ϵ_d respectively. If these materials are anisoropic, then in the final result, the dielectric constants are replaced by their geometric means. We now have, with $Q_m = Q/\epsilon$,

$$V^m(r,z) = \pi\int d^2q/(2\pi)^2[F(q)e^{-\gamma qz} + F'(q)e^{\gamma qz} + Q_m e^{-\gamma q|d-z|}]e^{iq\cdot r}/q,$$

$$V^u(r,z) = \pi\int d^2q/(2\pi)^2 G'(q)e^{(-q(z-d_1)+iq\cdot r)}/q,$$

while V^d remains the same. The boundary conditions at $z = 0$ becomes

$$F + F' + Q'_m = G, \tag{A9}$$

$Q'_m = Q_m\exp(-\gamma qd)$.

$$\epsilon/\epsilon_u(-F + Q'_m + F') = G.$$

Combining with Eq. (A9), we get

$$F + \beta_1 F' = -Q'_m\beta_1. \tag{A10}$$

$\beta_1 = (\epsilon_u - \epsilon)/(\epsilon_u + \epsilon)$ The boundary conditions at $z = d_1$ become

$$Fe^{-\gamma q d_1} + F' e^{\gamma q d_1} + Q''_m = G', \tag{A11}$$

$Q''_m = Q_m \exp[-\gamma q(d_1 - d)]$,

$\epsilon/\epsilon_d(-Fe^{-qd_1} - Q''_m + F'e^{qd_1}) = -(Fe^{-qd_1} + F'e^{qd_1} + Q''_m)$.

Combining with Eq. (A11), we get

$$\beta_2 F e^{-\gamma q d_1} + F' e^{\gamma q d_1} = -Q''_m \beta_2 \tag{A12}$$

$\beta_2 = (\epsilon_d - \epsilon)/(\epsilon_d + \epsilon)$. From Eqs (A10) and (A12), we get

$$F = -Q_m \beta_1 [\beta_2 e^{-\gamma q(d_1 - d)} - e^{\gamma q(d_1 - d)}]/det,$$

$$F' = Q_m \beta_2 [e^{-\gamma q(d_1 - d)} - \beta_1 e^{-\gamma q(d + d_1)}]/det,$$

$det = \beta_1 \beta_2 e^{-\gamma q d_1} - e^{\gamma q d_1}$. This solution is a generalization to anisotropic systems of Eq. (1) in Ref. [14]. The potential in units of Q is

$$G/Q_m = (F + F' + Q'_m)/Q_m = [-\beta_1 \beta_2 e^{-q(d_1 - d)} + \beta_1 e^{q(d_1 - d)}$$

$$+\beta_2 e^{-q(d_1 - d)} - \beta_1 \beta_2 e^{-q(d + d_1)}]/det + e^{-qd}.$$

We apply this to the screening of the BN potential. For the case with charge located at the interface so that $d = 0$, we get

$$G/Q_m = [-\beta_1 \beta_2 e^{-qd_1} + \beta_1 e^{qd_1}$$

$$+\beta_2 e^{-qd_1} - \beta_1 \beta_2 e^{-qd_1}]/det + 1.$$

When the film thickness is larger than the distance of interest, $qd_1 \gg 1$, $det \approx -e^{\gamma q d_1}$, $G/Q_m = \beta_1 e^{\gamma q d_1}/det + 1 = 1 - \beta_1$,

$$G = Q(1 - \beta)/\epsilon, \ (1 - \beta)/\epsilon = 1/\epsilon_{am} = 2/(\epsilon_1 + \epsilon). \tag{A13}$$

We obtain a very reasonable result expected from the effective medium approximation.

APPENDIX B: PHONON CALCULATION

We describe the calculation of the lattice dynamics [10] in this Appendix. We assume the lattice positions to be at $\mathbf{R}_i$. At each site, we write the in plane coordinates of the electrons and holes in terms of the center of mass equilibrium and fluctuation positions ($\mathbf{R}_i + \delta\mathbf{R}$) and the relative ($\mathbf{r}_i$) coordinates so that the coordinate of the ith electron is given by $\mathbf{r}_{ei} = \mathbf{R}_i + \delta\mathbf{R}_i + \mathbf{r}_i/2$; of the hole, $\mathbf{r}_{hi} = \mathbf{R}_i + \delta\mathbf{R}_i - \mathbf{r}_i/2$. The potential energy of interaction involves $U = \sum_{\alpha,\beta=e,h,i,j} V[(r_{\alpha,i} - r_{\beta,j})^2 + d^2\delta_{\alpha,\beta}]^{1/2}/2$, where $V(u) = e^2/u + V_B + V_N$ is sum of the Coulomb potential and the external potential due to the Boron and the Nitrogen ions at positions $\mathbf{R}_i^{B,N} + \delta\mathbf{R}_i^{B,N}$ with modulation $\delta\mathbf{R}_i^{B,N} = \sum_G \delta\mathbf{R}_G^{B,N} e^{i\mathbf{G}\cdot\mathbf{R}_i}$ from the interaction of the BN latice with the incommensurate TMDC lattice with reciprocal lattice vectors $\mathbf{G}$. We provide more details below of the derivations of these external potentials given in Eqs. (7) and (9).

The potential from the boron ions is given by the sum of the Coulomb potential over all the boron ions at positions $\mathbf{R}_i^B + \delta\mathbf{R}_i^B$: $V_B(r) = \sum_j U_B(r - \mathbf{R}_j^B - \delta\mathbf{R}_j^B)$. The Coulomb potential at transverse distance u and at vertical distance h from a single boron ion is given by $U_B(u) = Q_B \int d^2q/(2\pi)^2 \tilde{U}_q e^{iq\cdot u}$, $\tilde{U}(q) = \sum_h e^{-|q|h}/|q|/\epsilon_0/2$. Since $q \cdot \delta\mathbf{R}^B$ is small,

$$V_B(r) \approx V_{B1} + V_{B2},$$

$V_{B1} = \int d^2q/(2\pi)^2 \sum_j \tilde{U}_q e^{iq\cdot(r - \mathbf{R}_j^B)}$, $V_{B2} = \int d^2q/(2\pi)^2 \tilde{U}_q \sum_j e^{iq\cdot(r - \mathbf{R}_j^B)} iq \cdot \delta\mathbf{R}_j^B$. Substituting in the value $\delta\mathbf{R}_j^{B,N} = \sum_G \delta\mathbf{R}_G^{B,N} e^{i\mathbf{G}\cdot\mathbf{R}_j}$, we get $V_{B2} = \sum_G \delta \int d^2q e^{iq\cdot r}/(2\pi)^2 \sum_j \tilde{U}_q e^{i(G-q)\cdot\mathbf{R}_j^B} iq \cdot \delta\mathbf{R}^{GB})$. Performing the sum over j, we obtain for X=B, N; $V_{X1}^K(r) = \tilde{U}_K e^{i\mathbf{K}\cdot\mathbf{r}}/a_c$, $V_{X2}^{K-G}(r) = i\tilde{U}_{G-K} e^{i(\mathbf{G}-\mathbf{K})\cdot\mathbf{r}}[(\mathbf{G} - \mathbf{K}) \cdot \delta\mathbf{R}_G^X)]/a_c$; a_c is the area of the unit cell of the BN lattice.

The harmonic frequency is obtained from solving the phonon equation for the Fourier transform phonon modes:

$$m\omega^2 e_i(q) = \sum_j e_j(q) D_{ij}(q), \tag{B1}$$

where the dynamical matrix $D_{ab}(q) = \sum_{\mathbf{R}}(1 - \cos\mathbf{q}\cdot\mathbf{R})\nabla_a\nabla_b U(R)$, $e_i(q)$ is the polarization vector. The self-consistent phone frequencies obtained by replacing the dynamical matrix D by an average $\langle D\rangle$ so that $\langle D_{ab}(q)\rangle = \sum_{\mathbf{R}}(1 - \cos\mathbf{q}\cdot\mathbf{R})\nabla_a\nabla_b\langle U(R + \delta R)\rangle$. The angular brackets indicate a self-consistent thermal and quantum average over the fluctuation δR. We summarize the self-consistent phonon theory next.

1. The self-consistent phonon theory

The ground state self-consistent phonon wave function is a Gaussian which involves frequencies that are calculated from an averaged dynamical matrix $D_{\alpha\beta}^{scp}$:

$$\Psi(\xi_1, \ldots, \xi_N) \propto \exp\left(-\sum_{q\lambda}\left(\frac{m\omega_{q\lambda}}{2\hbar}\right)\xi_{q\lambda}\xi_{-q\lambda}\right), \tag{B2}$$

where $\xi_{q\lambda} = \sum_i 1/\sqrt{N}\, e^{-iqR_i}\, \vec{\xi}_i \cdot e_{q\lambda}$ is the normal mode coordinate.

This dynamical matrix itself is evaluated in the ground state of the system.

$$D_{\alpha\beta}^{scp}(q) = \sum_R \langle \nabla_{\alpha\beta}^{(2)} V(R + \xi)\rangle (1 - e^{iqR}). \tag{B3}$$

The ground state average is the average over $\xi_{q\lambda}$ having a gaussian distribution of width $(\hbar/2m\omega_{q\lambda})^{1/2}$, which is the mean square displacement of a 1D harmonic oscillator; more precisely, the average of any function F of the variable ξ is given by

$$\langle F(\xi(R))\rangle = \frac{det(\Lambda_R)^{\frac{1}{2}}}{2\pi}\int d^2\xi\, F(\xi)\, e^{-\frac{1}{2}\xi\,\Lambda_R\,\xi}, \tag{B4}$$

where

$$\left(\Lambda_R^{-1}\right)^{\alpha\beta} = \left\langle\left(\xi^\alpha(R) - \xi^\alpha(0)\right)\left(\xi^\beta(R) - \xi^\beta(0)\right)\right\rangle$$

$$= \frac{\hbar}{mN}\sum_{q\lambda}\frac{\mathbf{e}_{q\lambda}^\alpha\,\mathbf{e}_{q\lambda}^\beta}{\omega_{q\lambda}^0}\,(1 - \cos qR). \tag{B5}$$

So one can start from the set of quasi-harmonic frequencies of the solid, $\omega_{q\lambda}^0$ [obtained from Eq. (B3) with $\xi = 0$], use

them in Eq. (B5) to get $\Lambda^{\alpha\beta}$ to do the average in Eq. (B3), and diagonalize the self-consistent dynamical matrix to obtain new frequencies; these frequencies can themselves be used as input in Eq. (B5) and so on, until convergence of this iteration process. In Eq. (B4), the average of any odd function of ξ is zero, and in an expansion in powers of ξ only even powers contribute, since we are dealing with a gaussian average. The other point to notice is the physical interpretation of the matrix Λ. The expression of this matrix is very similar to the mean square displacements (MSD). In fact at very low temperatures, the MSD is just the trace of $\Lambda^{-1}_{R=a}$; therefore, it indicates the spreading of the particles about their lattice site. The average defined above is weighted by this spreading.

[1] A. Gamucci, D. Spirito, M. Carrega, B. Karmakar, A. Lombardo, M. Bruna *et al.*, Nat. Commun. **5**, 5824 (2014); M. Kellogg, J. P. Eisenstein, L. N. Pfeiffer, and K. W. West, Phys. Rev. Lett. **93**, 036801 (2004); E. Tutuc, M. Shayegan, and D. A. Huse, *ibid.* **93**, 036802 (2004); A. F. Croxall, K. Das Gupta, C. A. Nicoll, M. Thangaraj, H. E. Beere, and I. Farrer *et al.*, *ibid.* **101**, 246801 (2008); J. A. Seamons, C. P. Morath, J. L. Reno, and M. P. Lilly, *ibid.* **102**, 026804 (2009); J. P. Eisenstein, A. D. K. Finck, D. Nandi, L. N. Pfeiffer, and K. W. West, J. Phys.: Conf. Ser. **456**, 012009 (2013).

[2] For a recent reference, see S. T. Chui, *Physics of the Electron Solid* (International Press, Boston, 1994) and references therein.

[3] J. P. Eisenstein and A. H. MacDonald, Nature (London) **432**, 691 (2004); B. N. Narozhny and A. Levchenko, Rev. Mod. Phys. **88**, 025003 (2016); B. Debnath, Y. Barlas, D. Wickramaratne, and M. R. Neupane, R. K. Lake, Phys. Rev. B **96**, 174504 (2017); L. Rademaker, J. van den Brink, J. Zaanen, and H. Hilgenkamp, *ibid.* **88**, 235127 (2013).

[4] X. Liu, K. Watanabe, T. Taniguchi, B. I. Halperin, and P. Kim, Nat. Phys. **13**, 746 (2017); J. I. A. Li, T. Taniguchi, K. Watanabe, J. Hone, and C. R. Dean, *ibid.* **13**, 751 (2017); C. Zhang and G. Jin, J. Phys.: Condens. Matter **25**, 425604 (2013); K. Lee, J. Xue, D. C. Dillen, K. Watanabe, T. Taniguchi, and E. Tutuc, Phys. Rev. Lett. **117**, 046803 (2016).

[5] Z. Wang, D. A. Rhodes, K. Watanabe, T. Taniguchi, J. C. Hone, J. Shan, and K. F. Mak, Nature **574**, 76 (2019); See also, M. M. Fogler, L. V. Butov, K. S. Novoselov, Nat. Commun. **5**, 4555 (2014).

[6] R. A. Suris, J. Exp. Theor. Phys. **122**, 602 (2016).

[7] For parameters of bilayer graphene, see K. Zou, X. Hong, and J. Zhu, Phys. Rev. B **84**, 085408 (2011).

[8] The experiment we quoted in this paper with $2e^2/h$ plateau is fabricated using WSe_2 for both top and bottom layers. The experimental data for the effective masses are higher than the theoretical ones. For p-type holes in WSe_2, we have used the value of $0.8 - 0.9m_e$. See S. Xu, J. Shen, G. Long, Z. Wu, Z.-Q. Bao, C.-C. Liu, X. Xiao, T. Han, J. Lin, Y. Wu, H. Lu, J. Hou, L. An, Y. Wang, Y. Cai, K. M. Ho, Y. He, R. Lortz, F. Zhang, and N. Wang, Phys. Rev. Lett. **118**, 067702 (2017); However, an ARPES paper report the effective mass of WSe2 holes to be $1.4 \pm 0.6m_0$ at K valley and $3.5 \pm 1.8m_0$ at Γ valley, see P.-C. Yeh, W. Jin, N. Zaki, D. Zhang, J. T. Liou, J. T. Sadowski, A. Al-Mahboob, J. I. Dadap, I. P. Herman, P. Sutter, and R. M. Osgood, Jr., Phys. Rev. B **91**, 041407(R) (2015); M. V. Gustafsson, M. Yankowitz, C. Forsythe, D. Rhodes, K. Watanabe, T. Taniguchi, J. Hone, X. Zhu, and C. R. Dean, reported in K valley the relative effective masses for WSe2 of 0.45-0.55 (electrons) and 0.45-0.6 (holes) Nat. Mater. **17**, 411 (2018); We have used the electron effective mass of 0.5. For MoS2 (n-type), the effective mass is about $0.55m_e$, see J. Lin, T. Han, B. A. Piot, Z. Wu, S. Xu, G. Long, L. An, P. Cheung, P.-P. Zheng, P. Plochocka, X. Dai, D. K. Maude, F. Zhang, and N. Wang, Nano Lett. **19**, 1736 (2019); The theoretical band structures in TMDCs are described in G.-B. Liu, W.-Y. Shan, Y. Yao, W. Yao, and D. Xiao, Phys. Rev. B **88**, 085433 (2013); For some theoretical estimate of the masses, see A. Kormányos, G. Burkard, M. Gmitra, J. Fabian, V. Zólyomi, N. D. Drummond, V. Falâko, 2D Mater. **2**, 022001 (2015).

[9] N. Wang (private communication).

[10] L. K. Moleko, B. Joos, T. M. Hakim, H. R. Glyde, and S. T. Chui, Phys. Rev. B **34**, 2815 (1986).

[11] L. Chkhartishvili, S. Dekanosidze, N. Maisuradze, M. Beridze, R. Esiava, East.-Eur. J. Enterp. Technol. **3**, 50 (2015).

[12] E. P. Gross, Phys. Rev. **106**, 161 (1957); Ann. Phys. **4**, 57 (1958); A. F. Andreev and I. M. Lifshitz, Sov. Phys. JETP **29**, 1107 (1969); D. J. Thouless, Ann. Phys. **52**, 403 (1969); G. V. Chester, Phys. Rev. A **2**, 256 (1970); E. Kim and M. W. H. Chan, Science **305**, 1941 (2004); C. A. Burns, N. Mulders, L. Lurio, M. H. W. Chan, A. Said, C. N. Kodituwakku, and P. M. Platzman, Phys. Rev. B **78**, 224305 (2008); J. Day and J. Beamish, Nature (London) **450**, 853 (2007); S. Sasaki, R. Ishiguro, F. Caupin, H. J. Maris, and S. Balibar, Science **313**, 1098 (2006); A. S. C. Rittner and J. Reppy, Phys. Rev. Lett. **98**, 175302 (2007); M. Boninsegni, A. B. Kuklov, L. Pollet, N. V. Prokofev, B. V. Svistunov, and M. Troyer, *ibid.* **99**, 035301 (2007); J. Toner, *ibid.* **100**, 035302 (2008); L. Pollet, M. Boninsegni, A. B. Kuklov, N. V. Prokofev, B. V. Svistunov, and M. Troyer, *ibid.* **98**, 135301 (2007); S. T. Chui, Phys. Rev. B **82**, 014519 (2010).

[13] N. Wang *et al.* (unpublished).

[14] L. V. Keldysh, Sov. Phys. JETP Lett. **29**, 658 (1979).

[15] A. Chernikov, T. C. Berkelbach, H. M. Hill, A. Rigosi, Y. Li, O. B. Aslan, D. R. Reichman, M. S. Hybertsen, and T. F. Heinz, Phys. Rev. Lett. **113**, 076802 (2014).

[16] J. D. Jackson, *Classical Electrodynamics* (Wiley, New York, 1998).

[17] A. Laturia, M. L. Van de Put, and W. G. Vandenberghe, 2D Mater. Appl. **2**, 6 (2018).

[18] S. T. Chui and B. Tanatar, Phys. Rev. Lett. **74**, 458 (1995)

[19] For a displacement δa, the energy cost is $e^2(\delta a)^2/d^3 \approx (\delta a/d)^2 e^2/d \approx 4 \times 10^{-4} e^2/d$. This is much smaller than the pinning potential.

[20] F. C. Frank and J. H. Van Der Merwe, Proc. R. Soc. London A **198**, 205 (1949); **198**, 216 (1949).

[21] S. C. Ying, Phys. Rev. B **3**, 4160 (1971).

[22] In the small region close to the zone center, $|q| < [1 - (\gamma - \gamma_0)/\gamma]\pi/a$, the phonons are gapless and correspond to the movement of the misfit dislocations. These are absent in our approximation.

[23] R. Landauer, IBM J. Res. Dev. **1**, 223 (1957)

[24] M. Giradeau, J. Math. Phys. **1**, 516 (1960)

[25] M. Zarenia, D. Neilson, and F. M. Peeters, Sci. Rep. **7**, 11510 (2017) .

[26] D. Jerome, T. M. Rice, and W. Kohn, Phys. Rev. **158**, 462 (1967); L. Du, X. Li, W. Lou, G. Sullivan, K. Chang, J. Kono1, and R.-R. Du, Nat. Commun. **8**, 1971 (2017).

[27] For the wave function in real space form, see, for example, F. J. Dyson, J. Math. Phys. **8**, 1538 (1967).

[28] V. M. Asnin, A. A. Rogachev, and N. I. Sablina, Sov. Phys. JETP Lett. **11**, 99 (1970); C. Benoît à la Guillaume, M. Voos, and F. Salvan, Phys. Rev. B **5**, 3079 (1972)..

[29] W. F. Brinkman, T. M. Rice, P. W. Anderson, and S. T. Chui, Phys. Rev. Lett. **28**, 961 (1972); M. Combescot and P. Nozieres, J. Phys. C: Solid State Phys. **5**, 2369 (1972).

[30] S. T. Chui (unpublished).

[31] J. Jung, A. Raoux, Z. Qiao, and A. H. MacDonald, Phys. Rev. B **89**, 205414 (2014).

[32] J. M. Kosterlitz and D. J. Thouless, J. Phys. C: Solid State Phys. **6**, 1181 (1973)

[33] S. T. Chui and K. Esfarjani, Europhys. Lett. **14**, 361 (1991).

[34] E. J. Mele, Am. J. Phys. **69**, 557 (2001).